Intermodulation Read-Out Principle for Passive Wireless Sensors

Ville Viikari, *Senior Member, IEEE*, Heikki Seppä, and Dong-Wook Kim, *Member, IEEE*

Abstract—This paper presents a general intermodulation read-out principle for passive wireless sensors. A sensor utilizes a mixing element, such as a varactor, and it can be equipped with a capacitive, inductive, or resistive sensor element. When the sensor is illuminated with signals with two frequencies, it replies the sensor data at an intermodulation frequency. An analytical expression for the intermodulation response of the sensor is derived and verified by simulations. The concept is demonstrated at 1.2 GHz.

Index Terms—Mixers, RF identification (RFID), wireless sensors.

I. INTRODUCTION

WIRELESS sensors have a great deal of potential in numerous applications where a wired read-out is difficult, for example, due to harsh operating conditions, rotating parts, or cost and complexity of wiring. Wireless sensors are passive, battery-assisted semipassive, or active. The advantages of passive sensors are that their lifetime or operation conditions are not limited by the battery and that they are inexpensive.

Common passive wireless sensors are RF identification (RFID), surface acoustic wave (SAW) RFID, electrical resonance circuit sensors, and harmonic and intermodulation sensors. RFID is mostly used for identification, but will increasingly be used to realize sensors by adding a sensing element to the tag [1]–[3], and can also be used for telemetry [4]. The highest operation frequency and read-out distance of RFID are limited by the rectified power for the integrated circuit (IC) and are a few gigahertz and 5–10 m, respectively. An additional sensor element further increases power consumption.

SAW RFID tags transform an electromagnetic energy to SAWs propagating on a piezoelectric substrate. The SAWs are then manipulated and transformed back to electromagnetic waves. The SAW tags lend themselves well to sensors as the propagation properties of SAWs are inherently sensitive to several measured quantities such as temperature or strain and no external sensor element is needed. The SAW sensors in general are reviewed in [5] and [6] and some interrogation methods are described in [7] and [8]. The highest operation frequency is typically limited to several gigahertz by a minimum linewidth of acoustical reflectors fabricated on a substrate. In addition, a piezoelectric material as a sensing element may limit their applications.

Inductively coupled electrical resonance-circuit sensors are utilized to measure strain [9] and moisture [10]. These sensors consist of a simple electrical resonance circuit, whose resonance frequency is sensitive to the measured quantity, but they cannot be read across large distances as they require near-field coupling to a reader device.

Mixer sensors contain mixing elements such as diodes and transmit the sensor data either at a harmonic or intermodulation frequency when illuminated by a reader device. Although microwave illumination is usually used, an optical excitation signal can also be used for improved spatial localization [11].

Harmonic radar and tags were first proposed for traffic applications [12] and were used for tracking insects [13]–[15] and avalanche victims.[1] The intermodulation principle was first proposed for telemetry [16] and later was used to implement a wireless ferroelectric temperature sensor [17] and was modified for wireless microelectromechanical systems (MEMS) sensors based on mechanical mixing [18]. The advantage of the intermodulation principle over the harmonic scheme is a smaller frequency offset, which facilitates circuit design and compliance with frequency regulations. Generally, harmonic and intermodulation sensors can use a very high frequency and be operated at a large distance.

The intermodulation sensors in [17] and [18] utilize mixing elements (a ferroelectric varactor and MEMS resonator) as sensing elements and do not facilitate sensing elements in a straightforward way. In addition, proximity of dielectric or conductive material distorts the read-out of the ferroelectric intermodulation sensor.

We present an intermodulation read-out principle for passive wireless sensors in this paper. The read-out principle is tolerant of an electrical environment of the antenna and facilitates a generic capacitive, inductive, or resistive sensor element, such as a MEMS sensor. Potential applications of the sensor could include wireless monitoring of car tire pressure, moisture inside building structures, and strain in bridges. Ultimately, the concept could enable very small implantable health and fitness sensors.

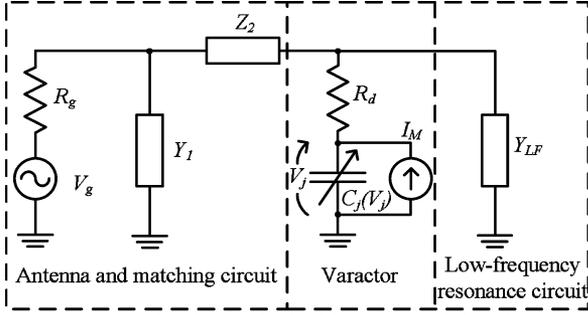[1][Online]. Available: www.recco.com

Fig. 1. Electrical equivalent circuit of the sensor consisting of an antenna (equivalent voltage generator), matching circuit, varactor diode, and low-frequency resonance circuit.

II. SENSOR

The sensor consists of an antenna (represented as a voltage source) matched to a mixing element, which is a varactor diode in this experiment, and a low-frequency resonance circuit containing a capacitive, inductive, or resistive sensing element, as shown in Fig. 1. In the following analysis, we consider a matching circuit consisting of a shunt admittance in parallel with the antenna and a series inductance between the antenna and the varactor although other matching topologies can be used as well.

The sensor is actuated with two signals at different frequencies. The signals are mixed in the varactor diode, which, among other frequencies, generates current at a difference frequency. The current at the difference frequency then generates a voltage that depends on circuit impedance. The voltage at the difference frequency further mixes with the original input frequencies, generating intermodulation signals. The low-frequency resonance circuit contains a sensor element that affects the impedance, and thus the voltage at the difference frequency. The sensor data is read out by recording the intermodulation response of the sensor.

In the following analysis, we derive a small-signal intermodulation response for the sensor. The derived response can be used to equate measured intermodulation responses to the sensor values and to predict the read-out range of the sensor.

A. Intermodulation Response of the Sensor

The antenna receives two frequencies and it produces a voltage of

$$V_g = 2\sqrt{2P_{in}R_g}(\sin \omega_1 t + \sin \omega_2 t)$$
$$= \hat{V}_g(\sin \omega_1 t + \sin \omega_2 t) \tag{1}$$

where P_{in} is a received power at one frequency, R_g is an antenna resistance, and ω_1 and ω_2 are angular frequencies of the sinusoids. Considering the circuit in Fig. 1, the voltage transfer

function from the antenna (generator) to the junction capacitance is shown in (2) at the bottom of this page, where $Y_d = 1/(R_d + 1/(j\omega C_{j0}))$ is a small-signal admittance of the diode, R_d is a series resistance of the diode, and C_{j0} is a junction capacitance at a zero bias. Let us consider an unbiased Schottky varactor diode. The junction resistance at a zero bias is typically very large ($\sim$ MΩ) and can be neglected. In addition, we assume no parasitic capacitance or series inductance for simplicity. The voltage-dependent junction capacitance of the varactor is given as

$$C_j(V_j) = \frac{C_{j0}}{\left(1 - \frac{V_j}{\Phi}\right)^\gamma} \tag{3}$$

where γ is the profile parameter for the depletion capacitance ($\gamma = 0.5$ for a uniformly doped junction) and Φ is a junction potential. The charge stored in the capacitor is given as

$$Q_j(V_j) = \int C_j(V_j)dV_j = \frac{\Phi C_{j0}}{1 - \gamma}\left(1 - \frac{V_j}{\Phi}\right)^{-\gamma+1} \tag{4}$$

where a possible constant charge is omitted. The second-order Taylor's approximation for the charge is

$$Q_j(V_j) \approx C_{j0}V_j + \frac{\gamma C_{j0}}{2\Phi}V_j^2. \tag{5}$$

The current of an equivalent Norton current source in parallel with the junction capacitance (shown in Fig. 1) is given as

$$I_j = \frac{dQ_j(V_j)}{dt} \approx j\omega C_{j0}V_j + j\omega\frac{\gamma C_{j0}}{2\Phi}V_j^2. \tag{6}$$

The first term represents a current of a normal (voltage-independent) capacitor, whereas the second term generates mixing products. The modulated current of the equivalent current generator is obtained by substituting (1) and (2) into (6),

$$I_{j,m} \approx j\omega\frac{\gamma C_{j0}\hat{V}_g^2}{2\Phi}(S_{jg}(\omega_1)\sin \omega_1 t + S_{jg}(\omega_2)\sin \omega_2 t)^2. \tag{7}$$

The current at the difference frequency $f_\Delta = f_2 - f_1$ is

$$I_j(\omega_\Delta) \approx j\omega_\Delta\frac{\gamma C_{j0}\hat{V}_g^2 S_{jg}(\omega_1)S_{jg}(\omega_2)}{2\Phi}\cos \omega_\Delta t. \tag{8}$$

The junction voltage at the difference frequency is given as

$$V_j(\omega_\Delta) = \frac{j\omega_\Delta C_{j0}\gamma\hat{V}_g^2 S_{jg}(\omega_1)S_{jg}(\omega_2)Z_N(\omega_\Delta)}{2\Phi}\cos \omega_\Delta t \tag{9}$$

where the impedance of the equivalent Norton current source is given as

$$Z_N = \frac{1}{j\omega C_{j0} + \frac{1}{R_d + \frac{1}{Y_{LF} + \frac{1}{Z_2 + \frac{1}{Y_1 + R_g}}}}}. \tag{10}$$

$$S_{jg} = \frac{V_j}{V_g} = \frac{Y_d}{j\omega C_{j0}[Z_2(Y_d + Y_{LF}) + 1 + R_g[Z_2 Y_1(Y_d + Y_{LF}) + Y_1 + Y_d + Y_{LF}]]} \tag{2}$$
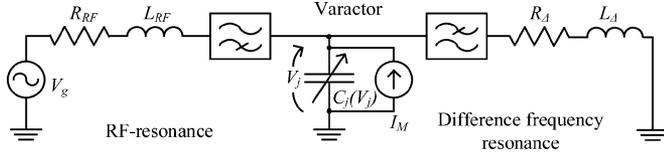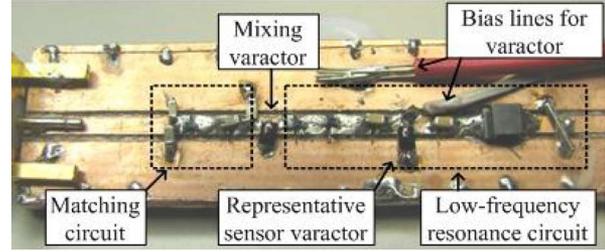
Fig. 2. Simplified equivalent circuit of the sensor.

Fig. 3. Photograph of the prototype sensor implemented with lumped elements soldered on a grounded 50-Ω coplanar waveguide.

The voltage at the difference frequency then mixes with the fundamental frequencies ω_1 and ω_2 generating intermodulation frequencies. The junction voltage at the intermodulation frequency $\omega_{IM} = 2\omega_1 - \omega_2$ is obtained by substituting (1), (9), and (10) into (6) as follows:

$$V_j(\omega_{IM})$$
$$= \frac{\omega_\Delta \omega_{IM} C_{j0}^2 \gamma^2 \hat{V}_g^3 S_{jg}^2(\omega_1) S_{jg}(\omega_2) Z_N(\omega_\Delta) Z_N(\omega_{IM})}{4\Phi^2}$$
$$\times \sin \omega_{IM} t. \tag{11}$$

The voltage transfer from the junction to the antenna is shown in (12) at the bottom of this page. Let us define the intermodulation response of the sensor as the ratio of the voltages at the intermodulation and fundamental frequencies across the antenna, shown in (13), at the bottom of this page.

Note that we omit the third-order term in the Taylor's approximation in (6). The third-order term would directly (without resonance at the difference frequency) generate currents at the intermodulation frequency. These currents do not depend on the resonance at the difference frequency and cannot be utilized for the sensor read-out. Equation (13) neglects these terms, although they likely occur in practice. Similarly, we have neglected the process in which the fundamental frequencies are first doubled in the varactor and are then mixed again with the fundamental frequencies to produce the intermodulation terms. The strength of intermodulation products generated in this process depends on the impedance of the equivalent Norton source given in (10) at the second harmonic frequencies $2\omega_1$ and $2\omega_2$, and this intermodulation production mechanism can be weakened with a proper circuit design. The intermodulation frequencies generated in this process are also practically independent of the difference frequency.

Equation (13) may be inconvenient due to its complexity. Let us consider the simplified equivalent sensor circuit consisting of two series *LCR*-resonators separated with ideal high- and low-pass filters, as shown in Fig. 2.

Repeating the previous analysis for the sensor of Fig. 2 gives an intermodulation response that is proportional to (under the assumption of $f_\Delta \ll f_{RF}/Q_{RF}$)

$$S_{IM} \sim \frac{Q_{RF}^4}{\left(Q_{RF}^2 \left(\frac{f_{0,RF}^2 - f_{RF}^2}{f_{0,RF}^2} \right) + \frac{f_{RF}^2}{f_{0,RF}^2} \right)^2}$$
$$\times \frac{Q_\Delta}{\sqrt{Q_\Delta^2 \left(\frac{f_{0,\Delta}^2 - f_\Delta^2}{f_{0,\Delta}^2} \right)^2 + \frac{f_\Delta^2}{f_{0,\Delta}^2}}} \tag{14}$$

where $Q_{RF} = 1/(2\pi f_{0,RF} R_{RF} C_{j0})$ and $Q_\Delta = 1/(2\pi f_{0,\Delta} R_\Delta C_{j0})$ are the quality factors of the two resonators at the carrier resonance frequency $f_{0,RF} = 1/(2\pi\sqrt{L_{RF}C_{j0}})$ and the difference resonance frequency $f_{0,\Delta} = 1/(2\pi\sqrt{L_\Delta C_{j0}})$. The model of Fig. 2 agrees well with that of Fig. 1 near the resonances. The simplified model also reveals that the intermodulation conversion efficiency is proportional to the fourth power of the quality factor of the RF resonator (or matching circuit) and directly proportional to the quality factor of the low-frequency resonator.

III. EXPERIMENTS AND SIMULATIONS

A. Sensor Prototype

The sensor prototype is implemented using lumped capacitors and inductors as matching elements and a varactor diode as a mixing element. The lumped elements are soldered on a grounded 50-Ω coplanar waveguide shown in Fig. 3.

We demonstrate a wireless sensor by adding a voltage-controlled varactor in the low-frequency resonance circuit. The voltage-controlled varactor simulates a general capacitive sensing element and its value is controlled with an external

$$S_{gj} = \frac{1}{R_d[Y_1 + 1/R_g + Y_{LF} + Y_{LF} Z_2 (Y_1 + 1/R_g)] + Z_2(Y_1 + 1/R_g) + 1} \tag{12}$$

$$S_{IM} = \frac{V_g(\omega_{IM})}{V_g(\omega_1)} = \frac{\omega_\Delta \omega_{IM} C_{j0}^2 \gamma^2 \hat{V}_g^2 S_{jg}^2(\omega_1) S_{jg}(\omega_2) S_{gj}(\omega_{IM}) Z_N(\omega_\Delta) Z_N(\omega_{IM})}{4\Phi^2} \tag{13}$$
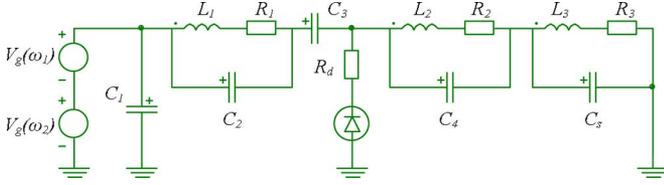
Fig. 4.   Schematic circuit of the simulation model.

TABLE I
PARAMETERS OF THE SENSOR USED IN THE
SIMULATIONS AND CALCULATIONS

Generator resistance	R_g = 50 Ω
Series resistance of L_1	R_1 = 0.62 Ω
Series resistance of varactor	R_d = 3 Ω
Series resistance of L_2	R_2 = 8 Ω
Series resistance of L_3	R_3 = 25 Ω
Matching inductor	L_1 = 11 nH
RF-block inductor	L_2 = 44 nH
Low-frequency inductor	L_3 = 4.7 μH
Matching capacitor	C_1 = 7.9 pF
Parallel capacitance of L_1	C_2 = 0.4 pF
Junction capacitance at zero bias	C_{j0} = 3 pF
Low frequency block capacitor	C_3 = 2.2 pF
Parallel capacitance of L_2	C_4 = 1.5 pF
Varactor capacitance at zero-bias	C_s = 4.3 pF
Parameter for the depletion capacitance	γ = 0.5
Junction potential	Φ = 0.87 V
Saturation current	I_s = 1 nA
Quality factor at the carrier frequency	Q_{RF} = 14.9
Quality factor at the difference frequency	Q_Δ = 24.0
Resonance at the carrier frequency	f_{RF} = 1.19 GHz
Resonance at the difference frequency	f_Δ = 23.76 MHz

dc-voltage source. The representative sensor varactor is identical to the mixer varactor.

B. Simulation Model

The intermodulation response of the sensor is simulated with the Aplac software (AWR, El Segundo, CA. [Online]. Available: http://web.awrcorp.com/) using the harmonic-balance simulation up to third harmonics. The mixing varactor is simulated using the Aplac diode model. The schematic circuit of the simulated sensor is shown in Fig. 4. The internal resistance of the voltage source is $R_g = 50$ Ω.

The matching admittance in the calculations is $Y_1 = j\omega C_1$, the matching impedance is

$$Z_2 = \frac{1}{j\omega C_2 + \frac{1}{R_1 + j\omega L_1}} + \frac{1}{j\omega C_3} \qquad (15)$$

and the low-frequency resonator admittance is

$$Y_{LF} = \frac{1}{\frac{1}{j\omega C_4 + \frac{1}{R_2 + j\omega L_2}} + \frac{1}{j\omega C_s + \frac{1}{R_3 + j\omega L_3}}}. \qquad (16)$$

The component values used in the simulations and calculations are summarized in Table I.

The nominal values of the inductors and matching capacitors are used in the simulations and calculations, but the inductor series resistances (R_1, R_2, R_3) and the parallel capacitances (C_2, C_4, C_s) are found out by fitting the theory to the measurements. The capacitance and series resistance of the mixing varactor are measured with a network analyzer.
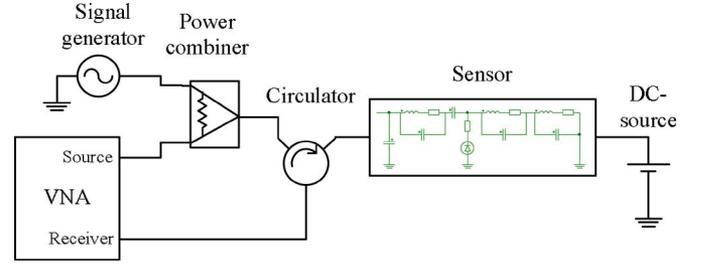

Fig. 5.   Schematic layout of the wired measurement setup for measuring the intermodulation response of the sensor.

The prototype sensor has two 1000-pF dc-block capacitors in series with C_s, and both varactors are shunted with 100-kΩ resistors to prevent unintentional charging. The dc-block capacitors and shunt resistors are excluded in the simulation model.

C. Measurement Setup

The intermodulation response is measured with a network analyzer (Agilent E8364B) capable of frequency offset measurements. One excitation signal is generated by the network analyzer's source and the other by an external signal generator (Agilent E83650B). The signals are combined with a power combiner (Narda 4321-2) and are fed to the sensor through a circulator (Western Microwave 3JC-1020). The reflected signal from the sensor is distinguished with the circulator and detected by the network analyzer's receiver. A dc-source (Agilent E3646A) is used for biasing the varactor that represents a capacitive sensing element. The wired measurement setup is shown in Fig. 5.

In addition to the cabled measurements, the sensor response is measured wirelessly. In the wireless setup, the sensor is equipped with a half-wavelength dipole antenna that is made of 500-μm-thick copper wire and whose total length is 138 mm. The excitation signals from the power combiner are fed to a horn antenna (Dorado GH1-12N). The receiver of the network analyzer is connected to an identical horn and the distance between the horn antennas and the sensor is 1 m.

IV. RESULTS

A. Intermodulation Response of the Sensor

The calculated, simulated, and measured (by cable) intermodulation responses as a function of the input signal frequency f_1 are shown in Fig. 6. The difference frequency is kept constant $f_\Delta = 23.75$ MHz, the input power is $P_{in} = -15$ dBm, and the bias voltage of the representative sensor capacitance is $V_{DC} = 0$ V.

The calculated [see (13)] and simulated intermodulation responses align almost perfectly and agree well with the measured response near the resonance (or impedance match) at 1.2 GHz. The calculated response from (14) also agrees well with that calculated from (13) near the resonance showing that the simple model characterizes the frequency behavior well.

The same responses as a function of the difference frequency are shown in Fig. 7. The input frequency is $f_1 = 1.2$ GHz, the input power is $P_{in} = -15$ dBm, and the bias voltage of the representative sensor capacitance is $V_{DC} = 0$ V.

Fig. 6. Calculated [(13): solid blue in online version, (14): dotted green in online version], simulated (dashed black), and measured (dashed–dotted red in online version) intermodulation responses of the sensor as a function of f_1. The input power is -15 dBm and frequency difference is $f_\Delta = 23.75$ MHz.
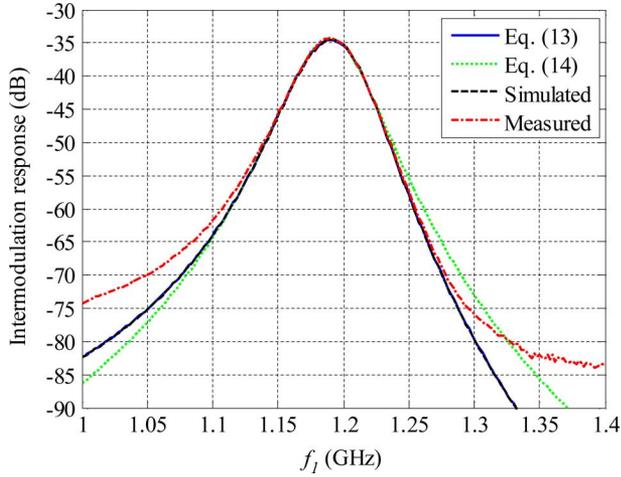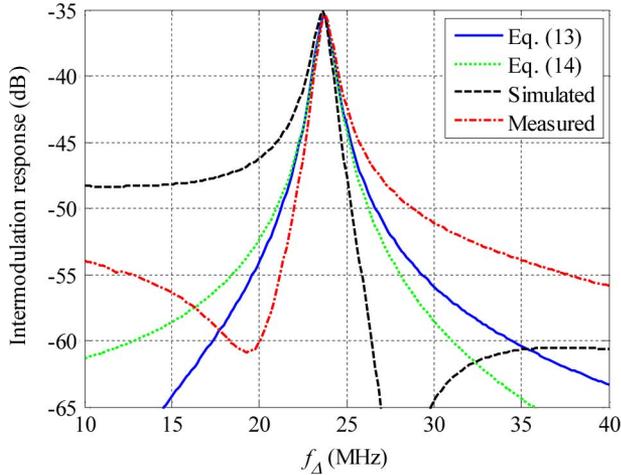

Fig. 7. Calculated [(13): solid blue in online version, (14): dotted green in online version], simulated (dashed black), and measured (dashed–dotted red in online version) intermodulation responses of the sensor as a function of f_Δ. The input power is -15 dBm and the input frequency is $f_1 = 1.2$ GHz.

The measured, calculated, and simulated responses are very similar at $f_\Delta = 23.75$ MHz, where $|Z_N|$ and the difference frequency-dependent intermodulation terms peak. The difference frequency-independent intermodulation terms (discussed in Section II-A) dominates outside this resonance, and therefore the analytic curves deviate from the measured and simulated curves. Recall that the difference frequency-independent intermodulation terms (the third-order voltage term in the Taylor approximation of (6) and the term produced when the second harmonic frequencies mix again with the fundamental frequencies) are neglected in the analysis.

The deviation between the measured and simulated curves is likely due to the phase at which the difference frequency-dependent and frequency-intermodulation terms add to each other. According to Fig. 7, these terms seem to add constructively below the resonance and destructively above the resonance in the simulation, whereas they sum in the opposite way in the measurements. This is likely due to parasitic elements that are
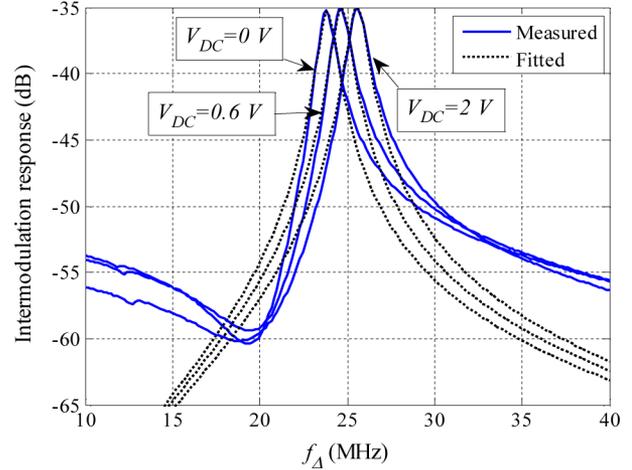

Fig. 8. Measured intermodulation responses at different bias voltages with the fitted analytical responses.

neglected in the simulations. The difference frequency-independent terms have a constant phase, whereas the phase of the difference frequency dependent term follows the impedance phase of the resonant circuit.

B. Sensor Response

The sensor principle is demonstrated by using a voltage-controlled varactor in the low-frequency resonance circuit representing a generic capacitive sensing element. The intermodulation response of the sensor is recorded at different bias voltages and the analytic model is fitted to the measured responses in order to find out the sensor capacitance values from the measured responses. Fig. 8 shows three measured intermodulation responses at bias voltages of 0, 0.6, and 2 V with the fitted analytical curves (13). A change in the sensor capacitance C_s shifts the resonance at the difference frequency.

The fitted sensor capacitance values from both wired and wireless measurements as a function of the bias voltage are depicted in Fig. 9. The results from both measurements coincide well to each other with the maximum difference of approximately 20 fF. The results verify that the sensor capacitance can also be determined wirelessly.

C. Power Dependency of the Sensor Response

The highest input power of the sensor is limited by the impedance of the mixing varactor that becomes power dependent at high power. The power dependency of the sensor response is studied by recording the intermodulation response at different power levels and determining the fitted sensor capacitance as a function of the input power. Three measured responses at the input power levels of -29, -19, and -9 dBm with fitted analytical responses (13) are shown in Fig. 10. The response shape remains almost unchanged at these power levels.

The measured sensor capacitance as a function of the input power is shown in Fig. 11.

Below -8 dBm, the absolute deviation of the measured sensor capacitance due to changing power is 10 fF from its low-power average. As the total sensor capacitance change in this experiment is 1.2 pF, the error due to unknown input power
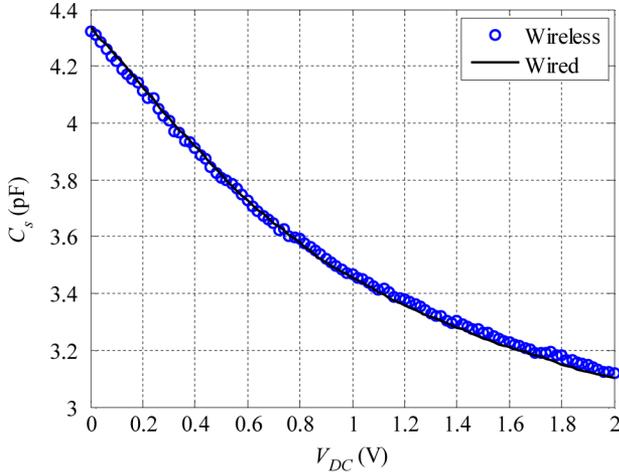
Fig. 9. Measured sensor capacitance wirelessly (blue circles in online version) and by cable (solid black line) as a function of the sensor varactor reverse bias voltage.
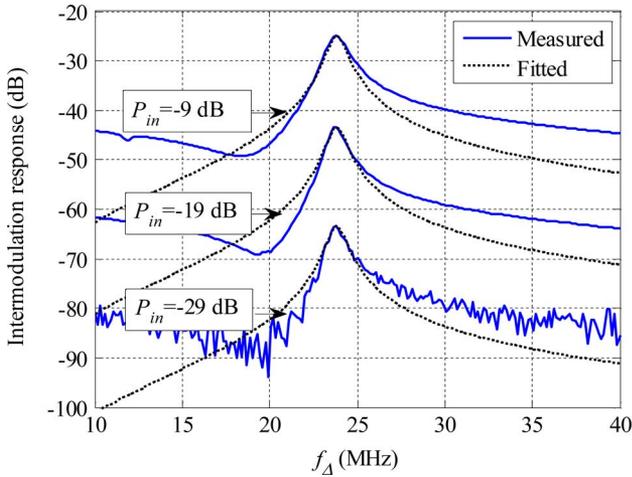

Fig. 10. Measured intermodulation responses at input power levels of -29, -19, and -9 dBm with the fitted analytical responses. The carrier frequency is $f_1 = 1.2$ GHz and the bias voltage is $V_{DC} = 0$ V.
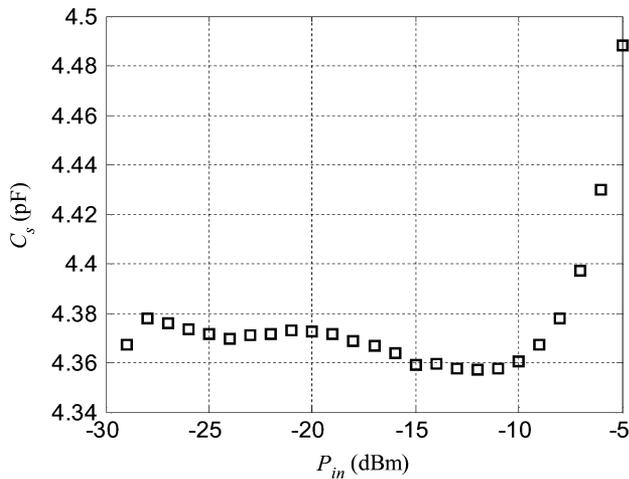

Fig. 11. Measured sensor capacitance as a function of the input power. The carrier frequency is $f_1 = 1.2$ GHz and the bias voltage is $V_{DC} = 0$ V.

below -8 dBm is only $\sim 0.8\%$. The measured sensor capacitance depends strongly on the input power above -8 dBm.

TABLE II
CALCULATED LINK BUDGET FOR THE PROTOTYPE SENSOR

Transmitted power	$P_t = 20$ dBm
Reader antenna gain	$G_r = 10$ dBi
Free space loss	$\left(\dfrac{4\pi r}{\lambda}\right)^2 = 53$ dB
Sensor antenna gain	$G_s = 3$ dBi
Received power by the sensor	$P_s = -20$ dBm
Intermodulation mixing loss	$L = 45$ dB
Sensor antenna gain	$G_s = 3$ dBi
Free space loss	$\left(\dfrac{4\pi r}{\lambda}\right)^2 = 53$ dB
Reader antenna gain	$G_r = 10$ dBi
Received power by the reader	$P_r = -105$ dBm

The power dependency of the sensor could possibly be reduced using a different mixing element. The power dependency could also be mitigated by measuring the sensor response at different power levels.

The difference between the measured sensor capacitances wirelessly and by a cable is of the same order (~ 20 fF) as the deviation due to unknown input power (~ 10 fF). Therefore, we assume that the measurement accuracy in this demonstration is not limited by the resolution.

D. Utilization as a Sensor

The proposed sensor platform can be used to implement a sensor by adding a capacitive, inductive, or resistive sensing element to the low-frequency resonance circuit. Examples of capacitive sensors are MEMS microphones [19], MEMS inertial sensors [20], MEMS pressure sensors [21], and ceramic humidity sensors [22]. The piezo-resistive strain gauges are widely used as deformation sensors and an inductive humidity sensor is presented in [10]. In addition, the demonstration readily shows how voltages can be measured wirelessly using a varactor. The voltage measurement accuracy in the wireless experiment is approximately 0.02 V and the tested range is 2 V. The piezoelectric strain gauge is an example of sensors producing a voltage output.

The read-out distance in the wireless experiment was 1 m, but the sensor could potentially be read-out across much larger distances. The read-out distance depends strongly on the intermodulation conversion efficiency, which for the demonstrated sensor is approximately -35 dB at -15-dBm input power level. The conversion efficiency is proportional to the squared input power in the small-signal region. The conversion efficiency could be increased using high-Q circuit elements and a mixing varactor with stronger capacitance–voltage nonlinearity.

Assuming that the prototype sensor was interrogated with a reader with 20-dBm transmit power, 10-dBi antenna gain, and -105-dBm sensitivity, and that the sensor was equipped with an antenna with 3-dBi gain, the detection distance of the sensor would be 9 m at 1.2 GHz. The corresponding link budget calculation is presented in Table II.

V. CONCLUSION

We have presented an intermodulation read-out principle for passive wireless sensors. The method enables wireless read-out

of a capacitive, inductive, or resistive sensing element. We have derived analytical equations for the intermodulation response of the sensor that can be used to calculate the sensor value from the measured response and to predict the achievable detection range. The analytical equations are verified by simulations and the concept is experimentally demonstrated at 1.2 GHz both wirelessly and by cable. This paper shows that it is feasible to implement passive wireless sensors based on the intermodulation principle.

REFERENCES

[1] R. Want, "Enabling ubiquitous sensing with RFID," *Computer*, vol. 37, no. 4, pp. 84–86, Apr. 2004.

[2] A. P. Sample, D. J. Yeager, P. S. Powledge, A. V. Mamishev, and J. R. Smith, "Design of an RFID-based battery-free programmable sensing platform," *IEEE Trans. Instrum. Meas.*, vol. 57, no. 11, pp. 2608–2615, Nov. 2008.

[3] C. Turcu, "Development and implementation of RFID technology," In-Teh, Vienna, Austria, 2009, pp. 89–178.

[4] V. Viikari, P. Pursula, and K. Jaakkola, "Ranging of UHF RFID tag using stepped frequency read-out," *IEEE Sens. J.*, vol. 10, no. 9, pp. 1535–1539, Sep. 2010.

[5] A. Pohl, "A review of wireless SAW sensors," *IEEE Trans. Ultrason., Ferroelect., Freq. Control*, vol. 47, no. 2, pp. 317–332, Mar. 2000.

[6] L. Reindl, G. Scholl, T. Ostertag, H. Scherr, U. Wolff, and F. Schmidt, "Theory and application of passive SAW radio transponders as sensors," *IEEE Trans. Ultrason., Ferroelect., Freq. Control*, vol. 45, no. 5, pp. 1281–1292, Sep. 1998.

[7] V. Viikari, K. Kokkonen, J. Meltaus, and H. Seppä, "Estimator for reflective delay line-type SAW sensors," *IEEE Trans. Ultrason., Ferroelec., Freq. Control*, vol. 56, no. 6, pp. 1277–1281, Jun. 2009.

[8] V. Viikari, K. Kokkonen, and J. Meltaus, "Optimized signal processing for FMCW interrogated reflective delay line-type SAW sensors," *IEEE Trans. Ultrason., Ferroelect., Freq. Control*, vol. 55, no. 11, pp. 2522–2526, Nov. 2008.

[9] J. C. Butler, A. J. Vigliotti, F. W. Verdi, and S. M. Walsh, "Wireless, passive, resonant-circuit, inductively coupled, inductive strain sensor," *Sens. Actuators A, Phys.*, vol. 102, no. 1–2, pp. 61–66, Dec. 2002.

[10] J. Voutilainen, "Methods and instrumentation for measuring moisture in building structures," D.Sc. dissertation, Dept. Elect. Commun. Eng., Helsinki Univ. Technol., Espoo, Finland, 2005.

[11] V. Viikari, J. Chisum, and H. Seppä, "Wireless passive photo detector for insect tracking," *Microw. Opt. Technol. Lett.*, vol. 52, no. 10, pp. 2312–2315, Oct. 2010.

[12] H. Staras and J. Shefer, "Harmonic radar detecting and ranging system for automotive vehicles," U.S. Patent 3 781 879, Jun. 30, 1972.

[13] E. T. Cant, A. D. Smith, D. R. Reynold, and J. L. Osborne, "Tracing butterfly flight paths across the landscape with harmonic radar," *Proc. R. Soc. B, Biol. Sci.*, vol. 272, no. 1565, pp. 785–790, Apr. 2005.

[14] J. R. Riley and A. D. Smith, "Design considerations for an harmonic radar to investigate the flight of insects at low altitude," in *Computers and Electronics in Agriculture*. Amsterdam, The Netherlands: Elsevier, 2002, vol. 35, pp. 151–169.

[15] B. G. Colpitts and G. Boiteau, "Harmonic radar transceiver design: Miniature tags for insect tracking," *IEEE Trans. Antennas Propag.*, vol. 52, no. 11, pp. 2825–2832, Nov. 2004.

[16] D. E. N. Davies and R. J. Klensch, "Two-frequency secondary radar incorporating passive transponders," *Electron. Lett.*, vol. 9, no. 25, pp. 592–593, Dec. 1973.

[17] V. Viikari, H. Seppä, T. Mattila, and A. Alastalo, "Wireless ferroelectric resonating sensor," *IEEE Trans. Ultrason., Ferroelect., Freq. Control*, vol. 57, no. 4, pp. 785–791, Apr. 2010.

[18] V. Viikari and H. Seppä, "RFID MEMS sensor concept based on intermodulation distortion," *IEEE Sens. J.*, vol. 9, no. 12, pp. 1918–1923, Dec. 2009.

[19] P. Rombach, M. Mullenborn, U. Klein, and K. Rasmussen, "The first low voltage, low noise differential silicon microphone, technology development and measurement results," *Sens. Actuators A, Phys.*, vol. A95, no. 2–3, pp. 196–201, Jan. 2002.

[20] N. Yazdi, F. Ayazi, and K. Najafi, "Micromachined inertial sensors," *Proc. IEEE*, vol. 86, no. 8, pp. 1640–1659, Aug. 1998.

[21] W. P. Eaton and J. H. Smith, "Micromachined pressure sensors: Review and recent developments," *Smart Mater. Structures*, vol. 6, no. 5, pp. 530–539, Oct. 1997.

[22] Z. M. Rittersma, "Recent achievements in miniaturised humidity sensors—A review of transduction techniques," *Sens. Actuators A, Phys.*, vol. 96, no. 2–3, pp. 196–210, Feb. 2002.

Ville Viikari (S'06–A'09–M'09–SM'10) was born in Espoo, Finland, in 1979. He received the Master's of Science (Tech.), Licentiate of Science (Tech.) (with distinction), and Doctor of Science (Tech.) (with distinction) degrees in electrical engineering from the Helsinki University of Technology (TKK), Espoo, Finland, in 2004, 2006, and 2007, respectively.

From 2001 to 2007, he was with the Radio Laboratory, TKK, where he studied antenna measurement techniques at submillimeter wavelengths and antenna pattern correction techniques. He is currently a Senior Research Scientist with the VTT Technical Research Centre, Espoo, Finland, and a Docent (equivalent to an Adjunct Professor) with Aalto University, Espoo, Finland. His current research interests are RFID systems and wireless sensors.

Dr. Viikari was the recipient of the IEEE Sensors Council 2010 Early Career Gold Award, the Young Scientist Award presented at the URSI XXXI Finnish Convention on Radio Science, Espoo, Finland (2008), and the Best Student Paper Award of the Annual Symposium of the Antenna Measurement Techniques Association, Newport RI (2005).

Heikki Seppä was born in Kortesjärvi, Finland, in 1953. He received the D.Sc. (Tech.) degree from the Helsinki University of Technology (TKK), Espoo, Finland, in 1989.

From 1976 to 1979, he was an Assistant with TKK, where he studied low-temperature physics and electrical metrology. In 1979, he joined the Technical Research Centre, Espoo, Finland, mainly to develop the quantum metrology. In 1989, he became a Research Professor with VTT. For several months during 1982–1983, he was with the National Institute of Standards and Technology (NIST), where he developed ultra low-temperature noise thermometer. In 2004, he was a Tutoring Professor in Nokia's Leading Science program. His research is focused on metrology, quantum devices, sensors, and especially on MEMS, wireless technology, and nanotechnology.

Dong-Wook Kim (S'93–M'00) received the B.S. degree in electronic communications from Hanyang University, Seoul, Korea, in 1990, and the M.S. and Ph.D. degrees in electrical engineering from the Korea Advanced Institute of Science and Technology (KAIST), Daejeon, Korea, in 1992 and 1996, respectively.

In 1996, he joined the LG Electronics Research Center, where he developed high-power devices and monolithic microwave ICs until 2000. From 2000 to 2002, he led research teams and developed integrated passive devices based on thick-oxidized Si substrate as a Research Center Director with Telephus Inc. From 2002 to 2004, he was also involved with the development of wireless security systems with the Samsung S1 Corporation. In 2004, he joined the faculty of Chungnam National University, Daejeon, Korea. In 2009, he was also with the Electronics and Telecommunications Research Institute (ETRI), as an Invited Researcher. In 2010, he was a Visiting Professor with the University of California at San Diego, La Jolla. His research interests are high-speed/high-frequency ICs and millimeter-wave modules including a miniaturized radar module, high-power module, and ultra-wideband module.